



PERGAMON

International Journal of Multiphase Flow 28 (2002) 527–552

---

---

International Journal of  
**Multiphase  
Flow**

---

---

www.elsevier.com/locate/ijmulflow

# Turbulence modulation by dispersed solid particles in rotating channel flows

Yingkang Pan <sup>1</sup>, Toshitsugu Tanaka <sup>\*</sup>, Yutaka Tsuji

*Department of Mechanophysics Engineering, Osaka University, Yamada-oka 2-1, Suita, Osaka 565-0871, Japan*

Received 17 April 2000; received in revised form 5 November 2001

---

## Abstract

Turbulence modulation in rotating channel flows due to small solid particles, at low particle volume fractions  $O(10^{-5})$ , is studied using direct numerical simulation (DNS).

It is found, for the larger and heavier particles in a rotating channel, that the consideration of inter-particle collisions in the modeling yields higher turbulence kinetic energy as compared to the one without consideration of the inter-particle collisions. From the present DNS results, it is shown that, the inter-particle collisions enhance the fluid turbulence energy in the central region mainly at low wavenumbers; the inter-particle collisions enhance the fluid turbulence energy in the near-wall regions in the whole spectral band.

The 70  $\mu\text{m}$  copper particles have a positive contribution in the vicinity of the pressure surface and a negative contribution a little far from it to  $\overline{u^2}$  and  $\overline{v^2}$ , while a negative contribution to  $\overline{uv}$  in the vicinity of the pressure surface. The dissipation and viscous diffusion are changed consequently in this area. When the inter-particle collisions have not been considered, the magnitudes of the peaks of terms in balance of the Reynolds stress equations are much damped near the pressure surface and their positions are moved away from the wall, and there is almost no gain or loss near the suction surface compared with the corresponding case considering the inter-particle collisions. Production term  $G_{12}$  due to system rotation plays an important role in the  $\overline{uv}$  equation, especially for the cases not considering the inter-particle collisions. © 2002 Elsevier Science Ltd. All rights reserved.

*Keywords:* Particles; Inter-particle collisions; Particle–turbulence interaction; Coriolis force; Rotating channel; Direct numerical simulation

---

<sup>\*</sup> Corresponding author. Tel.: +81-6-6879-7316; fax: +81-6-6879-7315.

*E-mail address:* tanaka@mech.eng.osaka-u.ac.jp (T. Tanaka).

<sup>1</sup> Present address: Technology Research Center, EBARA Research Co., Ltd., Fujisawa-shi 251-8502, Japan.

## 1. Introduction

The particle–turbulence interaction has become one of the most interesting topics in fluid mechanics because of new interesting phenomena and the many practical applications. Especially in a rotating system, the motion of particles is greatly affected by the Coriolis and centrifugal forces besides other forces (e.g. drag; Saffman lift force; Magnus force), so that particle's trajectories considerably deviate from the streamlines of the carrier fluid. The mechanism of the particle–turbulence interaction in a rotating system then becomes more complicated and interesting. Engineering applications are even more numerous, to mention a few: gas turbines operating with working fluids containing solid particles, induced fans for cleaning the dusts in a room.

Turbulence modification by particles will occur when the particle volume fraction reaches as  $O(10^{-5})$  for gas-particle/gas-droplet flows because of the density ratio of order of 1000, such that the momentum loss or gain to the turbulence by the particles is no longer negligibly small. There are many experimental investigations on turbulence modification by particles in jet, pipe and channel flow configurations (see the review by Tsuji, 1991). In general, large particles tend to increase the intensity of the fluid-phase turbulence, whereas small particles decrease it. Gore and Crowe (1989) reviewed the available experimental data on turbulence modification in gas–solid flows and suggested a critical parameter that predicts whether augmentation or suppression of the fluid-phase turbulence is  $d/l$ , where  $d$  is the particle diameter and  $l$  is the integral length scale of the turbulence. They got that the critical value is  $d/l \approx 0.1$ . Hetsroni (1989) suggested that particles with low particle Reynolds number,  $Re_p$ , suppress the turbulence, while particles with higher particle Reynolds number enhance the turbulence due to vortex shedding behind them. Yuan and Michaelides (1992) developed a simplified expression for the modification of turbulence intensity due to the presence of particles in dilute gas–solid flows. They examined two mechanisms; the energy dissipation due to the acceleration of a particle and the turbulence production due to particle wakes. Yarin and Hetsroni (1994) proposed another model based on the modified mixing-length theory and turbulent kinetic energy balance method for taking into account the carrier fluid velocity gradients and the turbulent wakes behind the coarse particles. Although both of their theoretical results showed fair agreement with the experimental data, they still left many questions regarding turbulence modification because of assumption based on ad hoc modeling.

Along with the development of supercomputers, DNS of the Navier–Stokes equations now becomes the most accurate computational approach to the problem since all essential scales of turbulent motions are resolved. Direct numerical simulations (DNS) including particle feedback (or called two-way coupling) on the fluid-phase turbulence appeared in the past decade. Squires and Eaton (1990) studied the turbulence modification by particles using DNS of isotropic turbulence. Only the Stokes drag was accounted in their DNS simulations. They found that the fraction of turbulence kinetic energy at high wavenumbers was increased relative to the energy at low wavenumbers for increasing values of the mass loading. They also found that the turbulence field was modified differently by light particles from by heavy particles because of the preferential concentration of the light particles in low-vorticity, high-strain-rate regions. Elghobashi and Truesdell (1993) investigated the effects of particle momentum response time, particle diameter, particle volume fraction and gravity on the turbulence structure in decaying homogeneous turbulence using DNS. They also got that the particles enhance the fluid turbulence energy at high wavenumbers and found that the particles transfer their momentum to the small-scale motion in

an anisotropic manner in gravitational environment. Moreover, they observed that the “cross-over” wavenumber decreases for the case in which gravity is strongest and decreases with time. McLaughlin (1994) presented a good review on the turbulence modification by dispersed particles. On the other hand, Pan and Banerjee (1997) conducted DNS with large particles and investigated the effects of large particles on wall turbulence. They found that the particles affect the ejection-sweep cycle near the wall, thereby increasing or decreasing the turbulence based on particle diameter. Their simulation was limited to the particle diameter larger than the Kolmogorov length scale and the higher particle volume fraction between  $O(10^{-3})$  and  $O(10^{-4})$ . In another way, Sundaram and Collins (1994a,b) developed a novel two-field formalism for calculating the two-point correlations and equivalent spectral densities for examining the particle–turbulence interaction. Very recently, Sundaram and Collins (1999) performed DNS of isotropic turbulence by suspended particles considering the inter-particle collisions with a hard-sphere collision model. They extended their formalism to compute the two-point energy correlations and spectra of the particle-laden flow field. They also observed that the particle inertia increases both the viscous and drag dissipations, and causes particle velocities to correlate for longer distance.

For the single-phase rotating channel flow, it is well known that the spanwise rotation affects both the mean motion and the turbulence structure. Bradshaw (1969) pointed out the similarity between rotation, streamline curvature, and thermal stratification on turbulent flows and defined an equivalent gradient ‘Richardson number’ to identify either a stabilizing or destabilizing effect on the flow subjected to system rotation. It was formally demonstrated by Johnston et al. (1972) by considering the simplified forms of the transport equations for the individual components of the Reynolds stress tensor. This essential issue has been elaborated by Tritton (1992) and Cambon et al. (1993). The spanwise roll cell instabilities due to system rotation were observed by Lezius and Johnston (1976) and Halleen and Johnston (1967). Lezius and Johnston (1976) also observed the large-scale cellular spanwise structures subjected to system rotation in their flow visualization. The single-phase turbulent rotating channel flow has been studied in detail by means of DNS by Kristoffersen and Andersson (1993). Their DNS results showed that, with increasing rotation rates, the augmentation and damping of the turbulence along the pressure and suction surfaces, respectively, became more significant, resulting in highly asymmetric profiles of mean velocity and turbulent Reynolds stresses; the vortices were shifted slightly towards the pressure surface with increasing rotation rates, and the number of vortex pairs therefore tends to increase with the rotation number  $Ro_\tau = \Omega H / u_\tau$ , where  $\Omega$  is the rotating speed,  $H$  is the channel half-width, and  $u_\tau$  is the friction velocity. Their DNS on the rotating shear flows reproduced many of the experimentally observed effects of the Coriolis forces on the mean flow and its turbulence structure. Zhou (1995) deduced a ‘role’ that relates the spectral transfer time to the eddy turnover time and the time scale for decay of the triple correlations on rotating turbulence. Canuto and Dubovikov (1997) extended their developed dynamical model for fully developed turbulence to encompass the presence of rotation. Cambon and Jacquin (1989) and Cambon et al. (1997) carried out a systematic study of the effect of rotation on the energy transfer by using the eddy damped quasi-normal Markovian (EDQNM) model. All above theoretical studies are based on isotropic turbulence or homogeneous turbulence of the single-phase rotating flow. Until now, the particle-laden rotating turbulent shear flow is still too difficult to deal with theoretically. The present DNS study on turbulence modification by the particles in rotating channel flows can provide some detailed information for further turbulence modeling.

The motion of particles in a rotating channel is extremely difficult to be observed experimentally in detail, even given today's sophisticated laser measurements. The group of Tabakoff (1984) had performed experimental and analytical investigations concerning the effects of the presence of solid particles on the performance of turbomachines. They had not considered the effects of particles and their inter-particle collisions on the fluid-phase turbulence. Because they applied an inviscid code for the fluid, the turbulence modification due to particles was impossible to be accounted for. The simplified rotating channel is regarded as a standard setting fundamentally studying on effects of Coriolis and centrifugal forces in turbomachines. In the previous study (Pan et al., 2000), we conducted the large-eddy simulation (LES) of particle-laden rotating channel flows at Reynolds number 250 and high rotation number up to 1.5 (both based on the friction velocity and the channel half-width), got that small and light particles accumulated in the region near the pressure surface depending on the rotation number; the inter-particle collision frequency becomes very high near the pressure surface due to the high local concentrations even at a low mean volume fraction  $O(10^{-5})$ ; small and light particles attenuate the contribution from the Coriolis forces to the turbulence and total turbulent kinetic energy of the carrier fluid, particularly in the near-wall regions. To investigate the particle-laden rotating channel flows at high resolution, Pan et al. (2001a) developed DNS of fully developed particle-laden rotating turbulent channel flows at the Reynolds number 194 and the rotation number 0.075. A  $128^3$  grid and the finite-difference method were applied for the carrier fluid. The dispersed particles were traced using a deterministic method based on equations of translational and rotational motions which are exact within certain formal limits containing the Coriolis and centrifugal forces. Hard-sphere collision model based on the impulsive force which is defined by the integral of the force acting on a particle versus time was applied to account for the particle interactions. The DNS results showed that inter-particle collisions make the lighter particles distribution more even and then attenuate the turbulence intensity of the fluid, and make the heavier particle distribution more uneven and then enhance the turbulence intensity of the fluid. It is also found that the little heavier particles (Stokes number  $St_\tau$  is 0.126) form strong streaky structures added "hooks" with a certain skew angle to the streamwise direction near the pressure surface.

In this study, we extend the previous work (Pan et al., 2001a) to analyze the energy spectrum and Reynolds stress terms, and to observe the turbulence modulation subjected to the existence of the dispersed particles and their inter-particle collisions in the fully developed rotating turbulent channel flows. Moreover, the mean velocity contours on the central cross-section are applied to study the modulation of the turbulence structure.

## 2. Mathematical description

### 2.1. Fluid field

Fig. 1 illustrates the coordinate system used to write the equations of motions for the carrier fluid and particles. A relative Cartesian coordinate system is employed here. The turbulent flow between two infinite parallel plates is driven by the pressure gradient in the streamwise direction and it rotates at a constant angular velocity in the spanwise direction. Here,  $x$  or  $x_1$  is the streamwise direction,  $y$  or  $x_2$  is the wall-normal direction, and  $z$  or  $x_3$  is the spanwise direction.

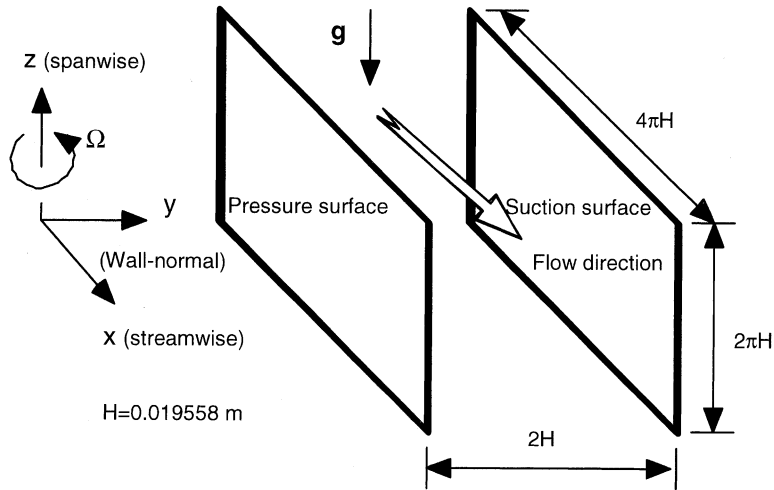


Fig. 1. Flow geometry and coordinate system.

Also,  $u$  or  $u_1$  is the streamwise velocity,  $v$  or  $u_2$  is the velocity in the wall-normal direction, and  $w$  or  $u_3$  is the velocity in the spanwise direction. Gravity acts downward in the negative  $z$  direction.

The fluid phase in a rotating channel is governed by the incompressible continuity and Navier–Stokes equations. The effect of particles on the continuity equation of the fluid is assumed negligible because of very low particle volume fraction  $O(10^{-5})$  in the present simulations. The effect of particles on the fluid momentum is accounted for in the Navier–Stokes equations with an external force field. The final governing equations can be expressed in the following forms:

$$\frac{\partial u_j}{\partial x_j} = 0, \tag{1}$$

$$\frac{\partial u_i}{\partial t} + \frac{\partial}{\partial x_j} (u_i u_j) = -\frac{\partial p_{\text{eff}}}{\partial x_i} + \frac{1}{Re_\tau} \frac{\partial^2 u_i}{\partial x_j \partial x_j} + 2\delta_{i1} + 2\varepsilon_{ij3} Ro_\tau u_j + F_{pi}, \tag{2}$$

where  $\delta_{ij}$  is the Kronecker delta symbol,  $\varepsilon_{ijk}$  is the Levi–Civita’s alternating tensor. The third term on the right-hand side in Eq. (2) is the dimensionless, gross downstream pressure gradient which would maintain a steady flow against the equilibrium, long-term wall friction produced by both boundaries. The fourth term on the right-hand side in Eq. (2) is the Coriolis force experienced by a fluid element resulting from system rotation. The effect of gravity on the fluid is assumed negligible because the fluid is assumed as air. The centrifugal force is conservative in nature (Johnston et al., 1972) and can be combined with the pressure gradient term

$$p_{\text{eff}} = p - \frac{1}{2} Ro_\tau^2 r^2, \tag{3}$$

where  $p$  is the normalized static pressure and  $r$  denotes the dimensionless distance from the axis of rotation.  $F_{pi}$  in Eq. (2) is the reaction of fluid force on particles contains in a unit mass of fluid element, which is given by

$$F_{p,i} = - \sum_{n=1}^N F_{n,i}, \quad (4)$$

where  $F_{n,i}$  is the instantaneous non-dimensionalized total forces acting on one particle  $n$ . Also,  $N$  is the instantaneous number of particles,  $N = N(x_1, x_2, x_3, t)$ , within the cell at which Eq. (2) is calculated. If we do the one-way coupling simulation,  $F_{n,i}$  is set to zero. Periodic boundary conditions are applied both in the streamwise  $x$  and spanwise  $z$  directions. The non-slip boundary conditions are imposed on the walls as

$$u_i = 0 \quad \text{at } y = 0 \quad \text{and} \quad y = 2H. \quad (5)$$

Eq. (2) is non-dimensionalized by the time-averaged mean wall friction velocity ( $u_\tau = \sqrt{\tau_w/\rho}$ ) and the channel half-width ( $H$ ). Based on this normalization, the Reynolds number is defined as  $Re_\tau = u_\tau H/\nu$ , and the rotation number as  $Ro_\tau = \Omega H/u_\tau$ , where  $\Omega$  is the angular velocity of rotation. In a stationary channel flow without rotation,  $u_\tau$  is the same on both walls of the channel, but this is not the case with rotation because of the asymmetry introduced by the Coriolis forces. If we define the time-averaged friction velocity on the stable side (suction surface) and unstable side (pressure surface) of the channel as  $u_{\tau s}$  and  $u_{\tau u}$ , respectively, then the following relationship can be obtained:

$$u_\tau^2 = \frac{1}{2} (u_{\tau s}^2 + u_{\tau u}^2). \quad (6)$$

The governing equations (1) and (2) were solved numerically using a semi-implicit method. The divergence form (2) we used is conservative for finite-difference schemes when a staggered grid is used. Spatial derivatives were approximated by a second-order accuracy central difference scheme. The advancement scheme for the velocity components  $u_i$  is a compact-storage third-order Runge–Kutta scheme published by Spalart et al. (1991) which has an explicit treatment for the convective terms and the source terms including the particle's feedback, and second-order-implicit Crank–Nicolson for the viscous term. This semi-implicit scheme seems suitable for the present cases because of its numerical stability and is regarded as a standard scheme in the DNS. An approximate factorization technique in three directions combined with the fractional step procedure (Kim and Moin, 1985) is used to get the prediction values of velocities. The fully developing flow under consideration is driven by an imposed mean pressure gradient, in the  $x$  direction, so that the turbulence may be treated as homogeneous in the streamwise ( $x$ ) and spanwise ( $z$ ) directions, i.e., mean properties and turbulence statistics vary only in the  $y$  direction normal to the plates. Therefore, the Poisson equation for pressure can be solved using Fourier series expansions in the streamwise and spanwise directions together with tridiagonal matrix inversion.

## 2.2. Particle motion

Although the mass loading ratio is on the order of unity, the particle volume fraction is still very low for most particle-laden rotating channel flows, especially in turbomachines. Lots of particles accumulate near the pressure surface (unstable side) because of the Coriolis forces. Therefore, the inter-particle collisions (including particle–wall collisions) take an important role in turbulence modulation in the rotating channels and should be considered (Pan et al., 2000).

Motion of a small rigid sphere in a turbulent flow field is described by a complicated equation by Maxey and Riley (1983). If all particles are rigid spheres with identical diameter  $d_p$  and density  $\rho_p$ , and the density of the particles is much larger than that of the carrier fluid, the equation of particle motion can be simplified in a rotating frame of reference with the axis of rotation aligned with the spanwise direction. It can be given in the following dimensional form:

$$m_p \frac{du_{pi}}{dt} = \frac{1}{2} \rho |\mathbf{u}_R| A \left[ C_D u_{Ri} + C_{LR} \frac{(\mathbf{u}_R \times \boldsymbol{\omega}_R)_i}{|\boldsymbol{\omega}_R|} \right] + f_{LG} \delta_{i2} - m_p g \delta_{i3} + \delta_{i1} m_p \Omega^2 r + 2\varepsilon_{ij3} m_p \Omega u_{pj}, \quad (7)$$

where  $m_p$  is the mass of a particle,  $u_{pi}$  the velocity of the particle in the  $x_i$  direction,  $\rho$  the density of the fluid, and  $A$  the projected area of the particle.  $\mathbf{u}_R$  and  $\boldsymbol{\omega}_R$  are, respectively, the relative velocity and rotation velocity vectors of the particle with respect to the fluid. The last two terms in Eq. (7) are the centrifugal force and the Coriolis force, respectively. Unlike the carrier fluid, the centrifugal force of the particle has no conservative nature. Those two extra forces enhance the inter-particle and particle–wall collisions and then affect the performance of the particle. The empirical relation for  $C_D$  that matches experimental data to within 5% up to particle Reynolds number  $Re_p = d_p |\mathbf{u}_R| / \nu$  of 800 (Schiller and Naumann, 1933) was employed, as

$$C_D = \frac{24}{Re_p} \left( 1 + 0.15 Re_p^{0.687} \right). \quad (8)$$

Rubinow and Keller (1961) derived the formula of the lift force developed due to rotation of the particle for Reynolds numbers at the order of unity. Until now, the lift force due to rotation of the particle for Reynolds numbers greater than 1 is still an open question. In the present simulations of the particle-laden rotating channel flows, the lift forces are much smaller than the drag and the gravity. The particle Reynolds number for the most simulated heavier particles is greater than 1. For the larger and heavier particles, the particle Reynolds number is greater than 10 frequently due to system rotation. Therefore, in the present simulations we employed the Rubinow–Keller lift coefficient  $C_{LR}$  for  $Re_p < 1$  and the lift coefficient  $C_{LR}$  for  $Re_p > 1$  according to Tsuji (1984). It can be expressed as

$$C_{LR} = \begin{cases} 2.0 \frac{d_p |\boldsymbol{\omega}_R|}{|\mathbf{u}_R|} & \text{for } Re_p \leq 1.0, \\ \min \left[ 0.5, 0.25 \frac{d_p |\boldsymbol{\omega}_R|}{|\mathbf{u}_R|} \right] & \text{for } Re_p > 1.0. \end{cases} \quad (9)$$

Saffman (1965, 1968) derived the formula of the lift force due to the velocity gradient on a particle for Reynolds numbers much less than unity. Recently, Cherukat et al. (1999) studied the inertial lift on a sphere in a linear shear flow field using a Fourier finite volume technique. They pointed out that Saffman’s formula overestimates the shear lift for  $Re_p > 1$ . On the other hand, the experiments of Hall (1988) showed that the predictions of Saffman are near the experimental data for the particle Reynolds number larger than 6 in a turbulent boundary layer. In addition, Tanaka and Tsuji (1991) found that the simulations considering the Saffman lift force had a good agreement of particle density distribution in a vertical pipe with their experimental data. So, the Saffman expression is employed here. In the present simulations, periodic boundary conditions were applied both in the streamwise and spanwise directions. Therefore, the mean velocity

gradients in those two directions can be regarded as negligibly small. The Saffman lift force was employed only in the wall-normal component with the expression as

$$f_{LG} = -1.62d_p^2 \rho u_{Rx} \sqrt{v \left| \frac{\partial u_{Rx}}{\partial y} \right| \left| \frac{\partial u_{Rx}}{\partial y} \right|}. \quad (10)$$

The equation of rotational motion of a particle is given by

$$I \frac{d\omega_{pi}}{dt} = -C_T \frac{1}{2} \rho \left( \frac{d_p}{2} \right)^2 |\omega_R| \omega_{Ri}, \quad (11)$$

where  $I$  is the moment of inertia of a particle. The right-hand side of Eq. (11) is the viscous torque against the particle's rotation, which is theoretically obtained by Dennis et al. (1980) and Takagi (1977).  $C_T$  is the non-dimensional coefficient determined by the rotational Reynolds number,  $Re_R = d_p^2 |\omega_R| / 4\nu$ . It can be expressed as

$$C_T = \frac{C_{T1}}{\sqrt{Re_R}} + \frac{C_{T2}}{Re_R} + C_{T3} Re_R. \quad (12)$$

The coefficients of  $C_{T1}$ ,  $C_{T2}$ , and  $C_{T3}$  are determined by  $Re_R$ . When  $Re_R < 10$ , we applied the values of  $C_{T1}$ ,  $C_{T2}$ , and  $C_{T3}$  by Takagi (1977). When  $Re_R > 10$ , we applied the values of  $C_{T1}$ ,  $C_{T2}$ , and  $C_{T3}$  by Dennis et al. (1980). This is summarized in Table 1. The momentum response time  $\tau_p$  is the time for momentum transfer due to drag and is calculated from

$$\tau_p = \left( \frac{4d_p}{3C_D} \right) \left( \frac{\rho_p}{\rho} \right) \frac{1}{|u_i - u_{pi}|} = \frac{d_p^2}{18\nu} \frac{\rho_p}{\rho} \frac{1}{(1 + 0.15Re_p^{0.687})}. \quad (13)$$

In the present simulations, the mean slip velocity between the fluid and the particles is applied in calculating the momentum response time  $\tau_p$ . The Stokes number  $St_\tau$  of the particles is defined as the ratio of the particle's momentum response time to the time scale of the carrier fluid

$$St_\tau = \frac{\tau_p}{H/u_\tau}. \quad (14)$$

Many time scales exist in the rotating turbulence flow. In the present simulations, the non-dimensional time unit ( $H/u_\tau$ ) is employed for simplicity. The translational velocity and the rotational velocity of a particle can be obtained by integrating Eqs. (7) or (11) using the second-order

Table 1  
Coefficients of particle rotation

$Re_R$	$C_{T1}$	$C_{T2}$	$C_{T3}$
$Re_R < 1$	0.0	$16\pi$	0.0
$1 < Re_R < 10$	0.0	$16\pi$	0.0418
$10 < Re_R < 20$	5.32	37.2	0.0
$20 < Re_R < 50$	6.44	32.2	0.0
$50 < Re_R < 100$	6.45	32.1	0.0

Adams–Bashforth explicit scheme, respectively. The position of a particle can be gotten according to velocity

$$u_{pi}^{(n+1)} = u_{pi}^{(n)} + \frac{\Delta t}{2} \left( 3H_{upi}^{(n)} - H_{upi}^{(n-1)} \right), \tag{15}$$

$$\omega_{pi}^{(n+1)} = \omega_{pi}^{(n)} + \frac{\Delta t}{2} \left( 3H_{\omega pi}^{(n)} - H_{\omega pi}^{(n-1)} \right), \tag{16}$$

$$x_{pi}^{(n+1)} = x_{pi}^{(n)} + \frac{\Delta t}{2} \left( u_{pi}^{(n)} + u_{pi}^{(n+1)} \right), \tag{17}$$

where  $H_{upi}, H_{\omega pi}$  are the sums of all terms on the right-hand sides of Eqs. (7) and (11), respectively. In the present simulations, a three-dimensional 8-node Lagrangian interpolation polynomial was used to obtain the velocities of the carrier fluid at the positions of the particles.

### 2.3. Inter-particle collision

Inter-particle collisions take an important role in the turbulence modification near the pressure surface in the rotating channel flows due to local particle concentrations. In the present situations, particle number density is so low that we applied the deterministic method (Tanaka and Tsuji, 1991). It is assumed that the particle volume fraction is so small that the binary collisions dominate in the present cases. Therefore, collision is mainly detected by calculating the distance of two particles' centers at the specific time when two particles collide with each other. Post-collision motion of the particle is described by the equations of impulsive motion as:

$$u_{pi}^* = u_{pi} + \frac{\mathbf{J}}{m_p}, \tag{18}$$

$$u_{pj}^* = u_{pj} - \frac{\mathbf{J}}{m_p}, \tag{19}$$

$$\omega_{pi}^* = \omega_{pi} + \frac{d_p}{2} \mathbf{n} \times \frac{\mathbf{J}}{I}, \tag{20}$$

$$\omega_{pj}^* = \omega_{pj} + \frac{d_p}{2} \mathbf{n} \times \frac{\mathbf{J}}{I}, \tag{21}$$

where  $\mathbf{J}$  is the impulsive force exerting on the particle  $i$  and  $\mathbf{n}$  is the normal unit vector directing from the center of the particle  $i$  to the contacting point.  $u_{pi}^*$  and  $u_{pj}^*$  are the post-collision velocities.  $\omega_{pi}^*$  and  $\omega_{pj}^*$  are the post-collision rotation velocities. Based on assuming spherical particles, a constant coefficient of restitution  $e$  and negligible particle deformation are assumed.  $\mathbf{J}$  is given by Tanaka and Tsuji (1991) in the following forms:

$$\mathbf{J} = J_n \mathbf{n} + J_t \mathbf{t}, \tag{22}$$

$$J_t = \min \left[ -\mu_p J_n, \frac{M}{7} |\mathbf{c}_s| \right], \tag{23}$$

$$J_n = (1 + e) M \mathbf{c} \cdot \mathbf{n}, \tag{24}$$

where  $\mathbf{t}$  is the tangential unit vector of the slip velocity from the particle  $j$  to the particle  $i$ .  $e$  is the coefficient of restitution.  $\mu_p$  is the coefficient of friction.  $M$  is equal to  $m_p$  for inter-particle collisions and  $2m_p$  for particle–wall collisions.  $\mathbf{c}$  is the relative velocity of mass center, and  $\mathbf{c}_s$  is the slip velocity at the contact point.

Particles were initially placed in random, non-contact positions in the rotating channel. The initial conditions of velocity fluctuations of the fluid were assumed by a random generator, the particle's initial velocities were assumed to be the same as the fluid velocities at the particle positions. The initial mean velocity along the  $y$  direction is assumed to the minimum of  $y^+$  and semi-logarithmic law distribution

$$U^+ = \min(y^+, 2.5 \ln y^+ + 5.5). \quad (25)$$

In all the numerical experiments the calculation domain used was  $4\pi H \times 2H \times 2\pi H$  in  $x$ ,  $y$  and  $z$  directions, respectively, which is same as that used by Kim et al. (1987). The calculation domain was divided into  $128^3$  computational cells with a uniformly spaced grid in the  $x$  and  $z$  directions ( $\Delta x^+ = 19.046$ ,  $\Delta z^+ = 9.523$ ) and a non-uniform grid distribution in the  $y$  direction ( $\Delta y_{\min}^+ = 0.292$ ,  $\Delta y_{\max}^+ = 7.104$ ) for  $Re_\tau = 194$ . The Reynolds number of the corresponding single-phase flow, based on the bulk mean velocity  $U_m$  (about 2.22 m/s) and the channel half-width  $H$ , was about 2900. In the present simulations a hyperbolic tangent transformation was used to generate the grid in the  $y$  direction. In the present simulations, the computational domain is assumed far from the axis of rotation. The inlet rotation radius of the domain is set to be large enough,  $r_0 = 50.41H$ , where  $H = 0.019558$  m, so that the computational domain is located in the experimental area of Johnston et al. (1972). Based on the above assumptions, periodic boundary conditions in the  $x$  and  $z$  directions for both the fluid and the particles were employed in the present simulations.

### 3. Results and discussion

In the present study, we investigate the turbulence modification due to the particles and the Coriolis forces in rotating channel flows. The simulations are done for cases with different particles, diameters and volume fractions. Three particle sets studied by Kulick et al. (1994) were simulated in the rotating channel. Particle properties of the different cases are listed in Table 2, in which  $\phi_v$  is the averaged volume fraction of the particles,  $\phi$  is the averaged mass loading ratio of

Table 2  
Particle properties for different cases

Case	$d_p$ ( $\mu\text{m}$ )	Material	$\rho_p$ ( $\text{kg/m}^3$ )	$\phi_v$ ( $10^{-6}$ )	$\phi$	$\tau_p$ (ms)	$St_\tau$	Inter-particle collisions
A	28	Lycopodium	700	1.52	0.0009	1.63	0.0124	Yes
B	28	Lycopodium	700	1.52	0.0009	1.58	0.0120	No
C	50	Glass	2500	8.65	0.0181	16.6	0.126	Yes
D	50	Glass	2500	8.65	0.0181	16.8	0.128	No
E	70	Copper	8800	23.74	0.1741	88.6	0.674	Yes
F	70	Copper	8800	23.74	0.1741	90.1	0.685	No

the particles, and the value of  $\tau_p$  is based on the averaged particle Reynolds number for the corresponding case. The averaged particle Reynolds numbers are 0.154 for case A, 0.334 for case B, 1.119 for case C, 0.948 for case D, 5.80 for case E, and 5.39 for case F, respectively. All of the simulated cases in Table 2 have the same particle number  $N_p = 156, 159$ . Cases A, C, and E have been considered the inter-particle collisions with a hard-sphere model. On the contrary, cases B, D, and F have not been considered the inter-particle collisions. Considering the inter-particle collisions, the dispersed particles are simulated in dimensionalized units. We set the coefficient of restitution  $e$  equal to 0.95 and the coefficient of friction  $\mu_p$  equal to 0.3 for all cases. The fluid is assumed as air with the properties ( $\nu = 1.5 \times 10^{-5} \text{ m}^2/\text{s}$ ,  $\rho = 1.2 \text{ kg/m}^3$ ) in the present simulations. The time step used in all the cases was 0.0008 non-dimensional time units ( $H/u_\tau$ ) for the fluid and the particle motion and 0.004 for the inter-particle collisions. These are much smaller than the particle momentum response time  $\tau_p$ , and so the particle motion can be assumed linear during one time step period. Before we started to simulate the particle-laden flows, a fully developed rotating channel flow field must have been prepared. First, to get the fully developed non-rotating channel turbulent flow field not influenced by the initial conditions, the flow field was advanced up to 28 non-dimensionalized time units. The simulated mean averaged values and the turbulence intensities were agreed well with the DNS results of Kim et al. (1987) using a spectral method. After that the fully developed rotating channel flow field at the rotation number 0.075 was obtained by conducting DNS in another 12 non-dimensional time units ( $H/u_\tau$ ). Second, each case of the particle-laden rotating channel flows listed in Table 2 was performed in another  $8H/u_\tau$  to reach the fully developed particle-laden rotating channel flow. After both the flow field and the particles had reached the statistically steady state, the equations were integrated further in time to get a running time average of the various statistical values. Almost all parts of the program for the fluid were vectorized. In the rest of the paper, the Reynolds number and rotation number  $Re_\tau, Ro_\tau$  will be referred to as  $Re$  and  $Ro$  for notational simplicity.

In the previous DNS study (Pan et al., 2001a), it is found that the inter-particle collisions of 70  $\mu\text{m}$  particles enhance the fluid turbulence due to their more uneven distribution compared to that without consideration of the inter-particle collisions. The DNS results also showed that the 50  $\mu\text{m}$  particles ( $St_\tau = 0.126$ ) form strong streaky structures added “hooks” with a certain skew angle to the streamwise direction near the pressure surface. When the particles become larger and heavier, and the particle volume fraction becomes higher  $O(10^{-5})$ , the well-known low/high speed streaks near the pressure surface are destroyed by the particles due to rotation. The present study tries to investigate the mechanism of turbulence modulation due to the dispersed particles using the statistical DNS results in a rotating channel.

### 3.1. Energy spectra

In the present simulations, the periodic boundary conditions were applied in the streamwise and spanwise directions both for the carried fluid and the dispersed particles. Therefore, the turbulence can be assumed to be homogeneous in those two directions, and the Taylor’s one-dimensional energy spectra can be applied to observe the turbulence modulation by the dispersed particles on the monitoring planes (Hinze, 1975; Kim et al., 1987). Three monitoring planes which are near the pressure surface  $y/(2H) = 0.0128$ , core region  $y/(2H) = 0.4908$ , and suction surface  $y/(2H) = 0.9855$ , respectively, were set to study the time-averaged quantities of the turbulence.

The monitoring planes close to the walls were so chosen because the turbulence intensities on those two planes in the wall-normal direction are near their peaks of the corresponding single-phase flow. The mean one-dimensional energy spectra can be obtained through the Fast Fourier Transform of the turbulence kinetic energy on each node on those planes and conventional averages over the other homogeneous direction and in time.

The small scales were found to deviate from local isotropy, primarily as a result of anisotropic transfer from the large scales in rotating turbulence with external forcing by Yeung and Zhou (1998) using DNS in a high resolution. In the rotating turbulence channel flows Kristoffersen and Andersson (1993) have not provided the one-dimensional energy spectra in their DNS results. From the present results, it is gotten that the small scales on the monitoring planes close to the walls of the single-phase flow demonstrate a obvious anisotropic property both in the  $x$  and  $z$  directions due to weak system rotation. On the other hand, it is also obtained that the energy spectra of large scales (at low wavenumbers) on the monitoring planes close to the suction surface are slightly larger than those close to the pressure surface.

It is very clear that inter-particle collisions in the turbulence flow will change the particle's instantaneous velocities then modify the turbulence. The mechanisms of the turbulence modification due to inter-particle collisions with external forcing are little known even with today's experimental apparatus. With the modern supercomputers, the inter-particle collisions in the turbulence flow are possibly simulated precisely within certain formal limits. The statistical DNS results show that the inter-particle collisions of the smaller and lighter particles (cases A and B) slightly attenuate the turbulence kinetic energy in whole spectrum along the two homogeneous directions except near the pressure surface along the  $x$  direction. Two turbulence kinetic energy components ( $E_{vv}$  and  $E_{ww}$ ) are little enhanced due to the inter-particle collisions at low wavenumbers near the pressure surface along the  $x$  direction. Significant changes of the turbulence modification due to the dispersed particles and their inter-particle collisions are detected when the particles become larger and heavier. Figs. 2 (cases C and D) and 3 (cases E and F) show the comparisons of the mean one-dimensional energy spectra along the streamwise direction between considering and not considering the inter-particle collisions. When the inter-particle collisions have not been considered, the statistical DNS results show that the larger and heavier particles (50  $\mu\text{m}$  glass or 70  $\mu\text{m}$  copper particles) attenuate the fluid turbulence intensities with the present mass loading. The inter-particle collisions of the larger and heavier particles relatively enhance the turbulence intensities according to Figs. 2 and 3 as pointed out in the previous work (Pan et al., 2001a). Furthermore, the turbulence kinetic energy components increase in whole spectrum except for the 70  $\mu\text{m}$  copper particles in the spanwise direction, and they are much enhanced at high wavenumbers near the walls [see Figs. 2(a), (c), 3(a) and (c)], and mainly increased at low wavenumbers in the central region [see Figs. 2(b) and 3(b)]. In other words, the inter-particle collisions of larger and heavier particles enhance the turbulence intensities in an anisotropic manner. This anisotropic feature of turbulence modification may be caused by the particle preferential concentration, the corresponding fluctuations of particle velocities, and the gravitational effect of particles. For the simulated largest and heaviest particles (70  $\mu\text{m}$  copper particles), the fluid turbulence intensity in the spanwise direction close to the pressure surface becomes greater than that in the streamwise direction because of the gravitational effect.

The results also demonstrate that the smaller and lighter particles (28  $\mu\text{m}$  Lycopodium particles) and their inter-particle collisions attenuate the turbulence kinetic energy component ( $E_{uu}$ )

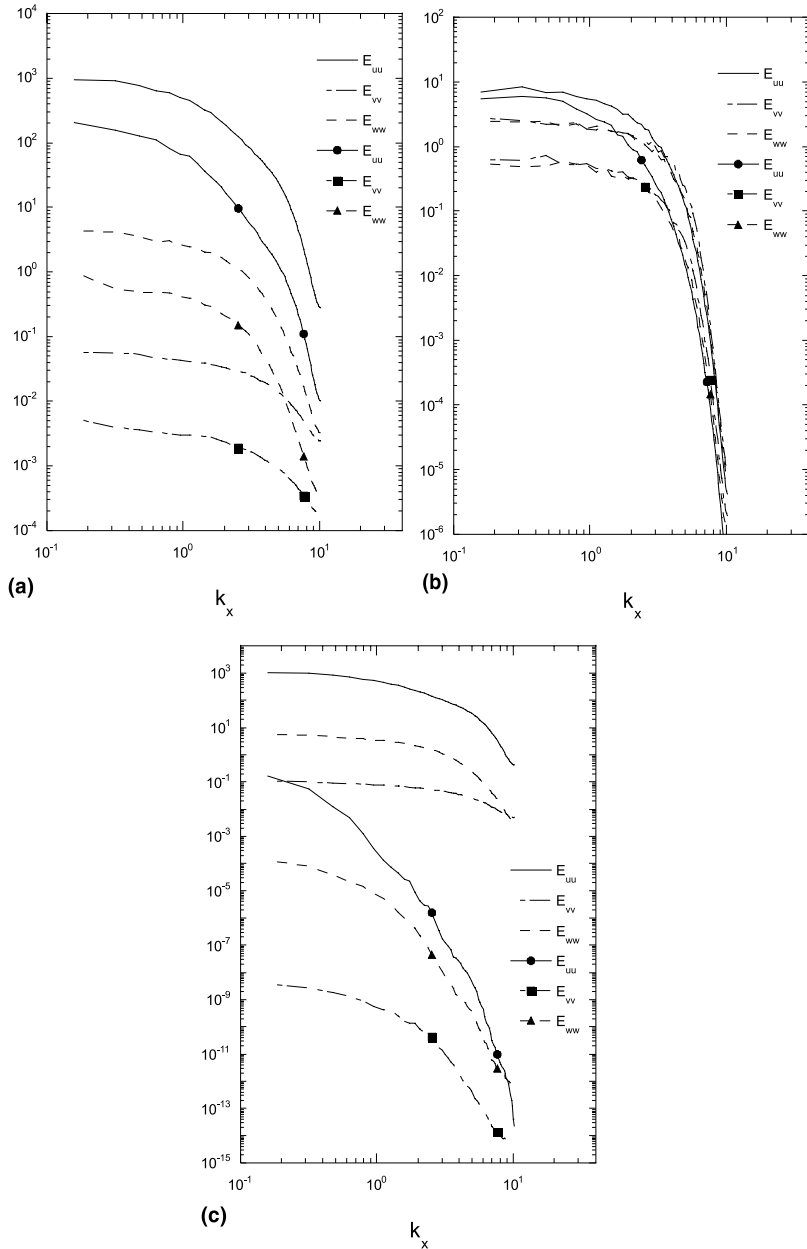


Fig. 2. Comparison of one-dimensional energy spectra along the streamwise direction between cases C and D (without symbols: case C; with symbols: case D): (a) near the pressure surface,  $y/(2H) = 0.0128$ ; (b) near core region,  $y/(2H) = 0.4908$ ; (c) near the suction surface,  $y/(2H) = 0.9855$ .

and slightly change other two components ( $E_{vv}$  and  $E_{ww}$ ) in whole spectrum close to the suction surface. Moreover, they increase the  $E_{vv}$  and  $E_{ww}$  in whole spectrum and decrease  $E_{uu}$  at low wavenumbers close to the pressure surface. The stabilization/destabilization of fluid turbulence on

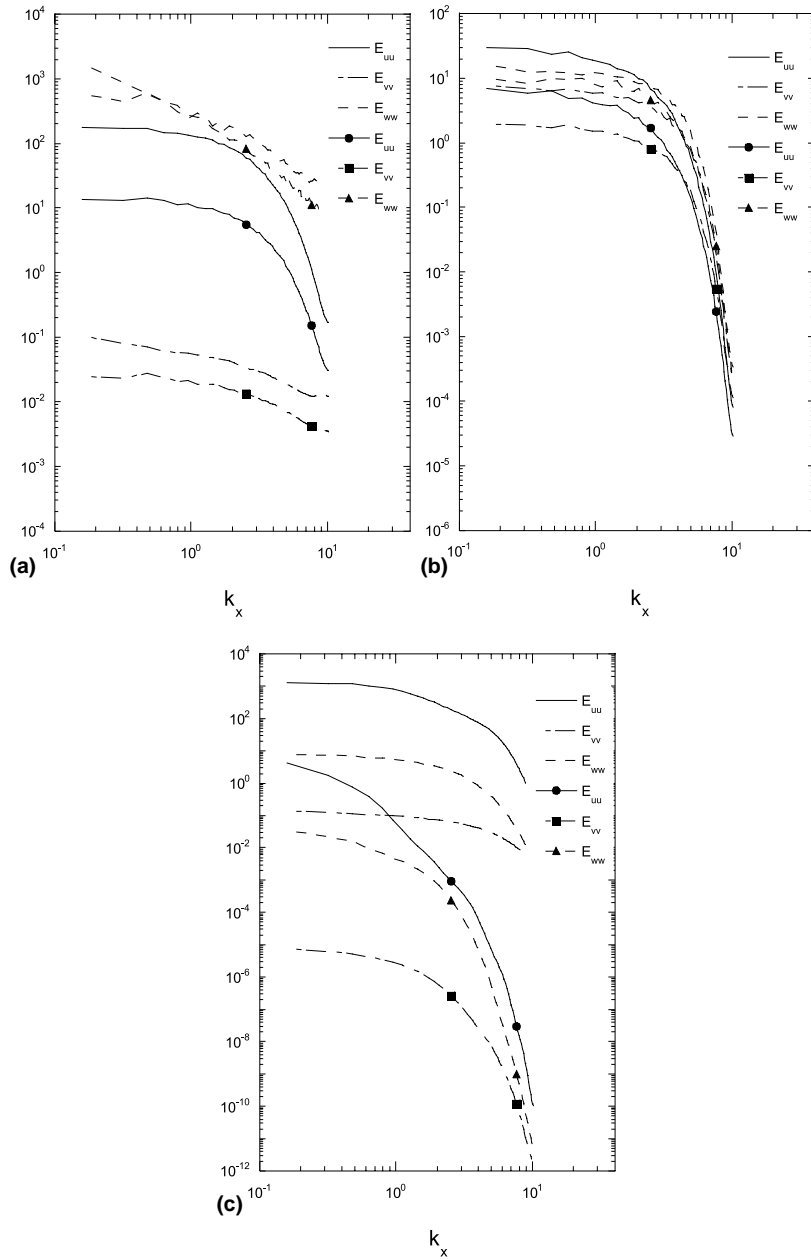


Fig. 3. Comparison of one-dimensional energy spectra along the streamwise direction between cases E and F (without symbols: case E; with symbols: case F): (a) near the pressure surface,  $y/(2H) = 0.0128$ ; (b) near core region,  $y/(2H) = 0.4908$ ; (c) near the suction surface,  $y/(2H) = 0.9855$ .

walls due to the Coriolis forces and the smaller and lighter particles can be obviously observed. Comparisons of the mean one-dimensional energy spectra between the single-phase flow and the case E considering the inter-particle collisions also have been done and shown in Fig. 4. When the

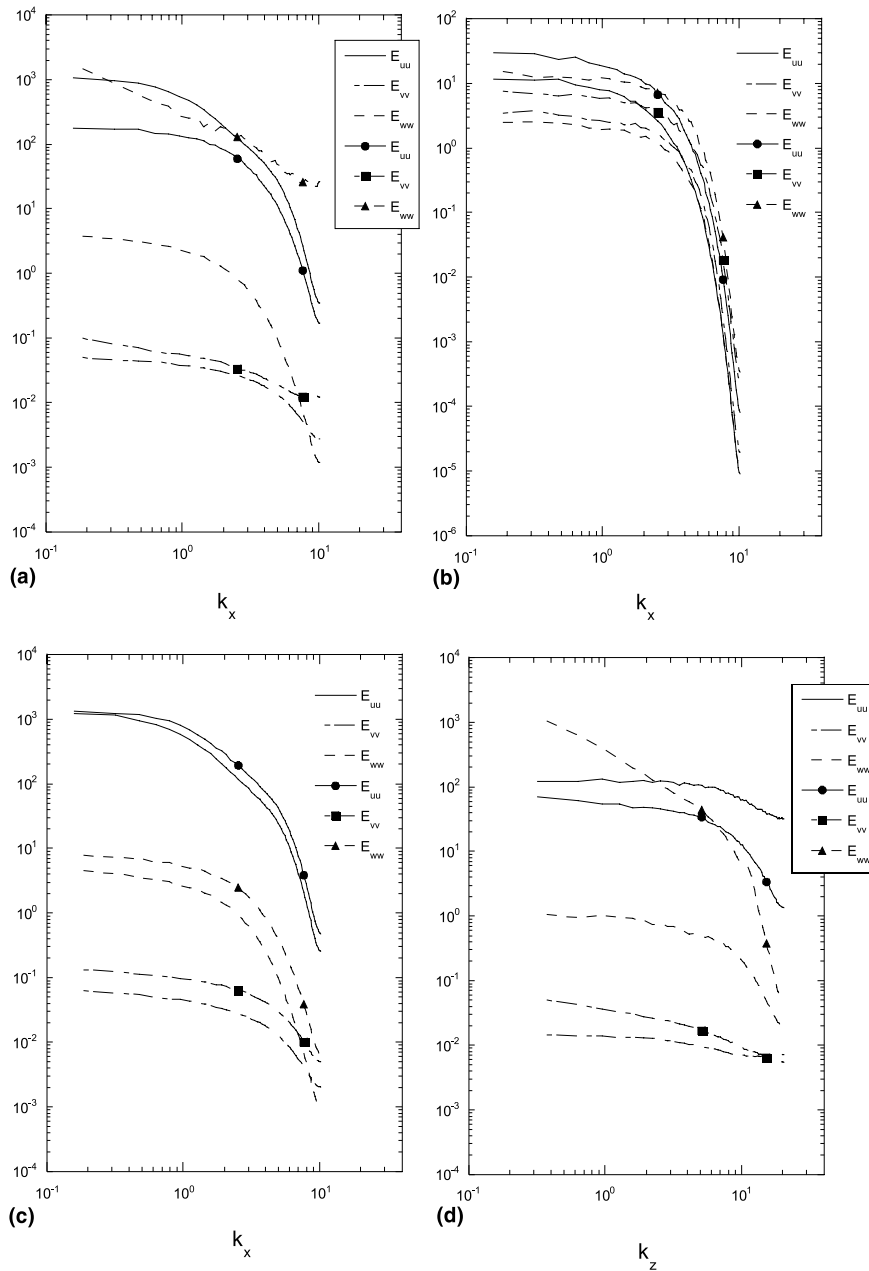


Fig. 4. Comparison of one-dimensional energy spectra along the streamwise and spanwise [(d) only] directions between single-phase flow and case E (without symbols: single-phase flow; with symbols: case E): (a) near the pressure surface,  $y/(2H) = 0.0128$ ; (b) near core region,  $y/(2H) = 0.4908$ ; (c) near the suction surface,  $y/(2H) = 0.9855$ ; (d) near the pressure surface,  $y/(2H) = 0.0128$ .

particles become larger and heavier, the particles and their inter-particle collisions significantly increase the turbulence kinetic energy close to the suction surface in whole spectrum, and they also

enhance  $E_{vv}$  and  $E_{ww}$  close to the pressure surface in whole spectrum, especially to the turbulence kinetic energy component  $E_{ww}$  at high wavenumbers in the  $x$  direction [see Fig. 4(a)] and at low wavenumbers in the  $z$  direction [see Fig. 4(d)] due to the gravitational effect of the largest and heaviest particles. Significant compression of  $E_{uu}$  close to the pressure surface is detected at low wavenumbers in the  $x$  direction and at high wavenumbers in the  $z$  direction to the largest and heaviest particles.

In a recent study (Pan et al., 2001b), it was found that in a rotating system the turbulence modulation subjected to small dispersed particles is strongly related to the ratio of the rotation time scale  $[1/(2\Omega)]$  to the particle momentum response time  $\tau_p$ ,  $Ro_p = 1/(2\Omega\tau_p)$ . The fluid–particle exchange rates of kinetic energy and dissipation can be obviously detected when  $Ro_p$  is small. Anisotropic effects of rotation of the single-phase rotating flow were studied in detail by Yeung and Zhou (1998) in their DNS at  $256^3$  resolution. In particle-laden rotating turbulent flows, the particle is more sensitive than the fluid to the Coriolis and centrifugal forces in a rotating system because of its inertia. Particle concentration and their interaction enhance this phenomenon and then have the anisotropic effects on the fluid turbulence. Pan et al. (2001b) also showed that the fluid and the particles were strongly correlated each other when  $Ro_p$  is small by observing the one-point velocity correlations between them. In the present DNS simulations, the rotation time scale  $[1/(2\Omega)]$  keeps constant 0.877 s for all the cases. The local turbulent time scales and particle momentum response time  $\tau_p$ , are different from place to place. For the cases with the glass or copper particles, the values of  $Ro_p$  are much smaller than that of the cases with the Lycopodium particles. Therefore, the effects of particles on the turbulence kinetic energy are significant and can be detected by observing the one-dimensional energy spectra.

### 3.2. Reynolds stress budgets

The effects of rotation on the Reynolds stress components are important in this work. The Reynolds stress equations of the single-phase flow, generalized to include system rotation, are given by Launder et al. (1987), and in simplified form by Johnston et al. (1972). A numerical study of the effects has been done in detail by Yeung and Zhou (1998) on a rotating isotropic turbulence. Following the equation derived by Launder et al. (1987), we can get the equation of the particle-laden rotating flow written for compactness in Cartesian tensor notation in the reference frame rotating with angular velocity  $\Omega$  about the  $z$ -axis in non-dimensional form as

$$\frac{D\overline{u_i u_j}}{Dt} = P_{ij} + G_{ij} + C_{ij} + D_{ij} + d_{ij} + \Phi_{ij} + \varepsilon_{ij} + Q_{ij}, \quad (26)$$

where

$$P_{ij} \equiv - \left\{ \overline{u_i u_k} \frac{\partial U_j}{\partial x_k} + \overline{u_j u_k} \frac{\partial U_i}{\partial x_k} \right\}, \quad G_{ij} \equiv 2Ro_\tau \{ \overline{u_j u_m} \varepsilon_{im3} + \overline{u_i u_m} \varepsilon_{jm3} \},$$

$$C_{ij} \equiv - \frac{\partial \overline{u_i u_j u_k}}{\partial x_k}, \quad D_{ij} \equiv \frac{1}{Re_\tau} \frac{\partial^2 \overline{u_i u_j}}{\partial x_k^2}, \quad d_{ij} \equiv - \frac{\partial}{\partial x_k} (\overline{p_{\text{eff}} u_i} \delta_{jk} + \overline{p_{\text{eff}} u_j} \delta_{ik}),$$

$$\Phi_{ij} \equiv \overline{p_{\text{eff}} \left( \frac{\partial u_i}{\partial x_j} + \frac{\partial u_j}{\partial x_i} \right)}, \quad \varepsilon_{ij} \equiv - \frac{2}{Re_\tau} \frac{\partial \overline{u_i}}{\partial x_k} \frac{\partial \overline{u_j}}{\partial x_k}, \quad Q_{ij} \equiv \overline{u_j F_{pi}} + \overline{u_i F_{pj}},$$

where the overbar indicates the conventional averages over the homogeneous planes and in time. The quantities  $P_{ij}$  and  $G_{ij}$  are the production terms associated with the mean shear and rotational stress generation, respectively. Kristoffersen and Andersson (1993) specially analyzed these two terms at different rotation numbers in their DNS of single-phase rotating channel flows. Because  $G_{kk}$  vanishes, there is no direct turbulence energy created by the system rotation.  $C_{ij}$  is the convective term, and  $D_{ij}$  is the viscous diffusion, and  $\varepsilon_{ij}$  is the dissipative correlation. In the present particle-laden flows,  $Q_{ij}$  represents the contribution of particles to the Reynolds stress

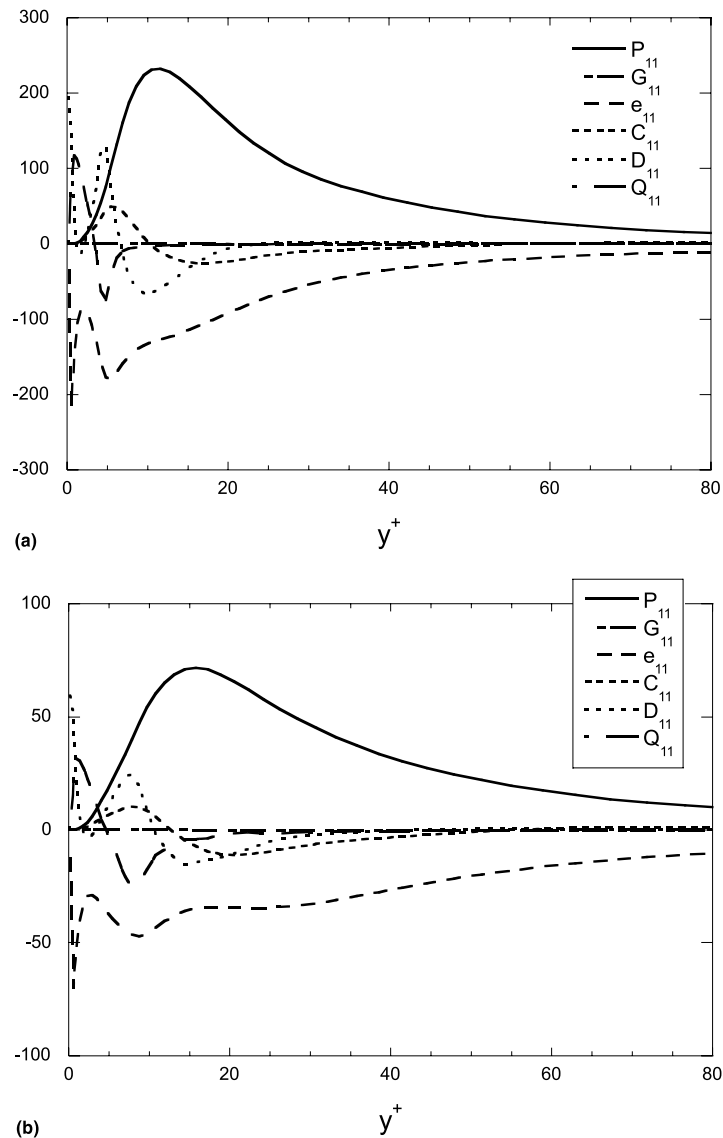


Fig. 5. Terms in balance of  $\overline{u^2}$  in local coordinates near the pressure surface: (a) case E; (b) case F.

components. For the single-phase flow,  $Q_{ij}$  is equal to zero. The turbulent stress diffusion process ( $d_{ij}$ ) and the pressure–strain process ( $\Phi_{ij}$ ) have not been analyzed in this study for simplification.

In the previous work (Pan et al., 2000), an attempt was done for accounting the effects of the finite-sized particles on the total production terms  $P_{ij} + G_{ij}$  using the LES of particle-laden rotating channel flows. The LES results showed that the 28  $\mu\text{m}$  Lycopodium particles attenuate the contribution from the Coriolis forces to the production terms, especially in the region close to the

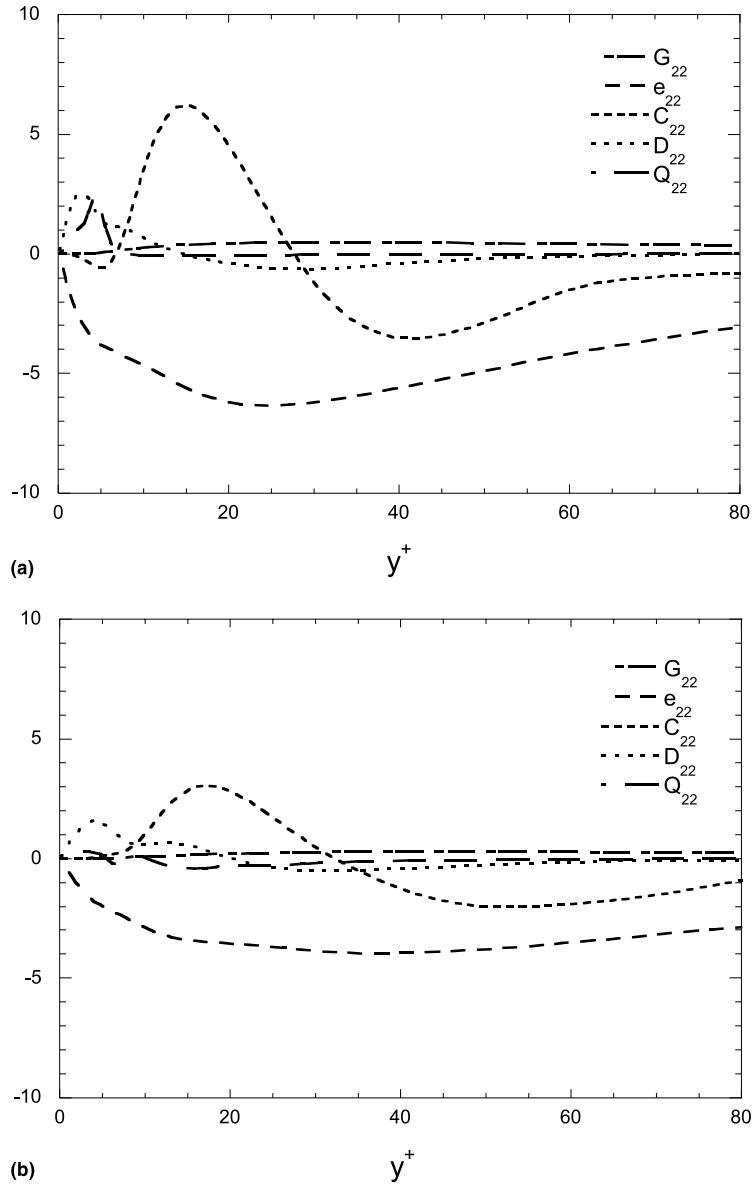


Fig. 6. Terms in balance of  $\overline{v^2}$  in local coordinates near the pressure surface: (a) case E; (b) case F.

pressure surface. Because of the weak rotation, the present 28  $\mu\text{m}$  Lycopodium particles have slightly changed the Reynolds stress components from the single-phase flow, therefore, the results are not discussed here. In Figs. 5–8 comparisons of the various terms in Eq. (26) of the rotating flow with 70  $\mu\text{m}$  copper particles between considering and not considering the inter-particle collisions are plotted in local wall coordinates near the pressure surface. All the  $Q_{ij}$  components are negligibly small except for cases E and F in the region close to the pressure surface. The production terms  $G_{ij}$  in the  $\overline{u^2}$  equations are so small compared with other terms that they can be neglected due to weak rotation.

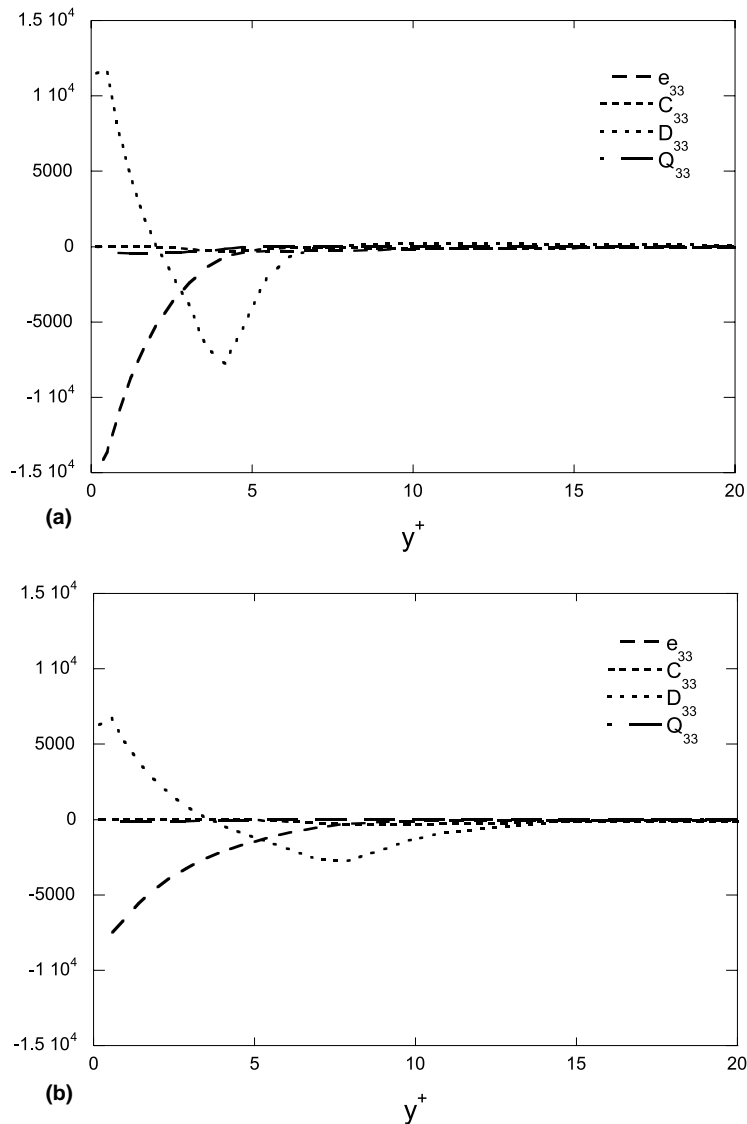


Fig. 7. Terms in balance of  $\overline{w^2}$  in local coordinates near the pressure surface: (a) case E; (b) case F.

The statistical DNS results show that the  $\overline{u^2}$  equation is largely dominated by production and dissipation. For case C containing the 50  $\mu\text{m}$  glass particles and considering the inter-particle collisions, there is a large peak in production near the wall ( $y^+ \approx 10$ ), which is balanced in part by the large dissipation near it. In the vicinity of the wall the large values of dissipation are balanced by the convective term and the viscous diffusion. Furthermore, all the magnitudes of the peaks near the pressure surface are slightly larger than those near the suction surface. This is similar to the DNS results of the curvature in wall-bounded turbulent flows by Moser and Moin (1987). On the other hand, there is almost no gain or loss near the suction surface of case D without con-

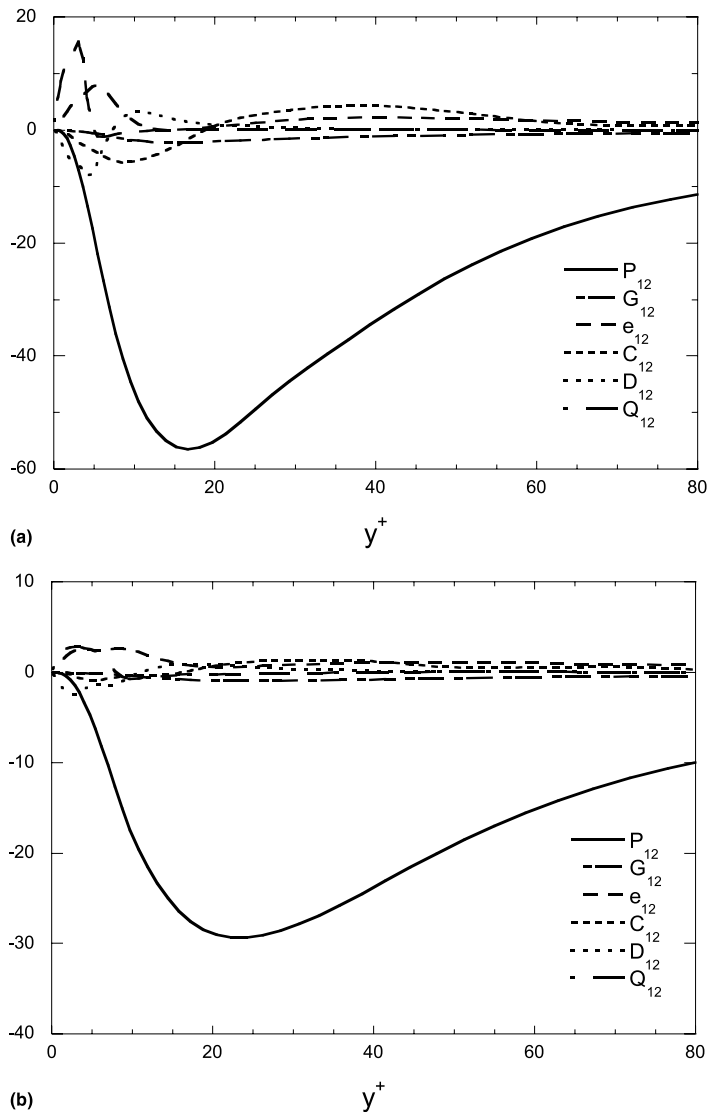


Fig. 8. Terms in balance of  $\overline{u^2}$  in local coordinates near the pressure surface: (a) case E; (b) case F.

sideration of the inter-particle collisions. All the magnitudes of the peaks near the pressure surface are also significantly damped and their positions move away from the walls. In addition, the large peak value in production decreases from about  $P_{11} \approx 260$  to  $P_{11} \approx 70$  and its position moves from  $y^+ \approx 10$  to  $y^+ \approx 20$  in the local wall coordinates. For case E containing the 70  $\mu\text{m}$  copper particles and considering the inter-particle collisions [see Fig. 5(a)], there is a large peak in production near the wall ( $y^+ \approx 10$ ). In contrast to case C, it is found that all the magnitudes of the peaks close to the pressure surface are significantly smaller than those close to the suction surface. It is also found that the simulated 70  $\mu\text{m}$  copper particles have made a positive contribution in the vicinity of the pressure surface ( $y^+ < 3.3$ ) and a negative contribution a little far from it ( $y^+ > 3.3$ ) to the Reynolds stress component  $\overline{u^2}$  explicitly. They also affect the dissipation  $\varepsilon_{11}$  and viscous diffusion  $D_{11}$  which have two peaks close to the pressure surface, respectively. In Fig. 5(b), in the same way, there is almost no gain or loss near the suction surface of case F. All the magnitudes of the peaks close to the pressure surface are also significantly damped and their positions move away from it. In addition, the large peak value in production decreases from about  $P_{11} \approx 230$  to  $P_{11} \approx 70$  and its position moves from  $y^+ \approx 10$  to  $y^+ \approx 15$  in the local wall coordinates.

Since  $P_{22} = P_{33} = 0$  there is no direct production of either  $\overline{v^2}$  and  $\overline{w^2}$ , their only source of energy is the pressure–strain correlation. The direct effects of system rotation are shown to reduce  $\overline{v^2}$  near the suction surface since  $G_{22} < 0$  and to increase  $\overline{v^2}$  near the pressure surface since  $G_{22} > 0$  from Fig. 6, as well as pointed by Kristoffersen and Andersson (1993). For case C, close to the wall there is a large convection from the normal component  $\overline{v^2}$  to the other components. Furthermore, the peak value near the suction surface is slightly larger than that near the pressure surface. This was observed by Moin and Kim (1982) in their computations of plane-channel flow and was referred to as the ‘splating’ or impingement effect. For the case E [see Fig. 6(a)], very close to the wall ( $y^+ < 7$ ) the convective term has a negative value, and near the position  $y^+ \approx 15$  there is a large convection from the normal component  $\overline{v^2}$  to the other components. In contrast to case C, the magnitude of the peak near the suction surface is slightly smaller than that near the pressure surface. It is also found that the simulated 70  $\mu\text{m}$  copper particles have made a positive contribution in the vicinity of the pressure surface ( $y^+ < 8$ ) and a negative contribution a little far from it ( $y^+ > 8$ ) to the Reynolds stress component  $\overline{v^2}$  explicitly. For case D or F not considering the inter-particle collisions, the 50  $\mu\text{m}$  glass or 70  $\mu\text{m}$  copper particles have similar effects on  $\overline{v^2}$  as on  $\overline{u^2}$  compared to the results of case C or E.

Fig. 7 shows the comparison of terms in balance of  $\overline{w^2}$  between cases E and F. For case E, in the vicinity of the wall there are significant viscous diffusion and dissipation. The magnitudes of the peaks near the pressure surface are significantly larger than those near the suction surface. In addition, in Fig. 7(a) the viscous diffusion has a peak value  $D_{11} \approx -7765$  near the position  $y^+ \approx 4$  for case E. For case F not considering the inter-particle collisions in Fig. 7(b), the magnitude of the peak is significantly damped. Furthermore, the viscous diffusion has a peak value  $D_{11} \approx -2772$  near the position  $y^+ \approx 8$  close to the pressure surface.

The direct effects of (positive) system rotation are expected to increase the negative level of  $\overline{w^2}$  near the pressure surface, and to reduce  $\overline{w^2}$  near the suction surface since  $G_{12} = -2Ro_\tau(\overline{u^2} - \overline{v^2}) < 0$  in the whole region. Fig. 8 shows the comparison of terms in balance of  $\overline{w^2}$  between cases E and F. From the previous work (Pan et al., 2000), the total production term  $P_{12} + G_{12}$  of the rotating channel flow with 28  $\mu\text{m}$  Lycopodium particles was significantly suppressed at a high rotation number compared with the corresponding single-phase flow. Significant

changes on Reynolds stress terms of  $\overline{uv}$  can be observed from the present results between considering and not considering the inter-particle collisions for the simulated 50  $\mu\text{m}$  glass or 70  $\mu\text{m}$  copper particles. In the present  $\overline{uv}$  equation, the production dominates, and again there is convective term and viscous diffusion from the maximum source region ( $y^+ \approx 15$ ) towards and away from the wall. However, for cases E and F in the vicinity of the pressure surface ( $y^+ < 5$  for case E and  $y^+ < 8$  for case F) the particle term  $Q_{12}$  contributes a positive value to  $\overline{uv}$  against the production term. However, in the present cases the viscous dissipation is negligible almost everywhere, and the production is balanced by the velocity–pressure-gradient and diffusion terms. For case F, all the terms are suppressed significantly and their peak positions move little far from the walls, and  $G_{12}$  plays a more important role in balance.

From the above analysis, it is seen that, for the larger and heavier particles in a rotating channel, particles and their interaction due to local concentration have direct contributions to the Reynolds stress budgets in the region near the pressure surface. Other terms in the Reynolds stress budgets are changed consequently. The anisotropic effects of the particles are then correlated with that of the fluid. The stabilization/destabilization effects in the rotating channel enhance the anisotropy of the fluid turbulence. Because the particles have no direct contribution to the Reynolds stress budgets and turbulent large scales dominate in the central area, particles and their interaction only can change the turbulent kinetic energy components at large scales (low wavenumbers).

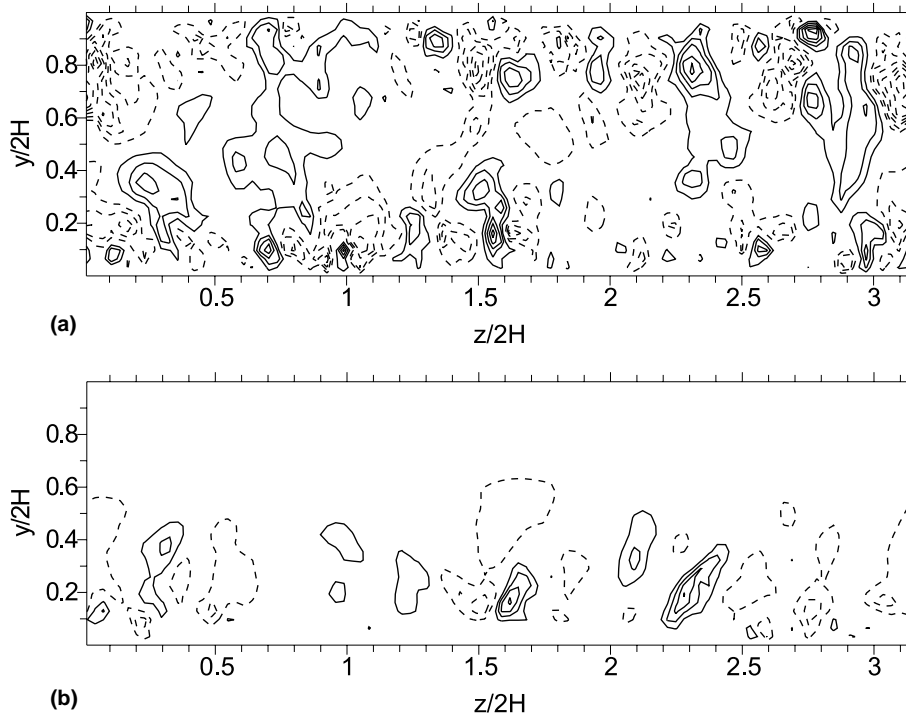


Fig. 9. Contours of secondary flow component  $\tilde{v}$  in the  $(y, z)$ -plane averaged over  $8H/u_\tau$ . Contour levels incremented by  $\pm 0.5$ , starting  $\pm 0.5$ . Dashed contours are negative. (a) Case C; (b) case D.

### 3.3. Turbulence structure

The so-called Taylor–Goertler vortices in the rotating channel flows firstly were observed experimentally by Johnston et al. (1972) and were also detected in the LESs of Kim (1983) and Miyake and Kajishima (1986a,b). Furthermore, this phenomenon was investigated in detail in DNS of Kristoffersen and Andersson (1993). At a high rotation number, they found that two pairs of counter-rotating vortices fill most of the cross-section, being shifted slightly towards the pressure surface. Such kinds of Taylor–Goertler vortices were also studied by Moser and Moin (1987) in their DNS of the curvature in wall-bounded turbulent flows. The pairs of counter-rotating vortices were also represented in a single-phase rotating channel at a high rotation number using the present DNS technique. According to Kristoffersen and Andersson (1993) and Moser and Moin (1987), the secondary-flow components  $\tilde{v}$  and  $\tilde{w}$  averaged in the streamwise direction and in time remained functions of  $y$  and  $z$  because of rotation or curvature. After averaging over  $8H/u_\tau$ , the effects of the particles and their interaction on secondary-flow components are obtained. In the present simulations, only  $\tilde{v}$  is applied because the effects on  $\tilde{w}$  are difficult to analysis due to the present weak rotation.

Figs. 9 and 10 show the comparisons of secondary flow component  $\tilde{v}$  in the  $(y,z)$ -plane averaged over  $8H/u_\tau$  among the different cases. The solid and dashed lines denote positive and

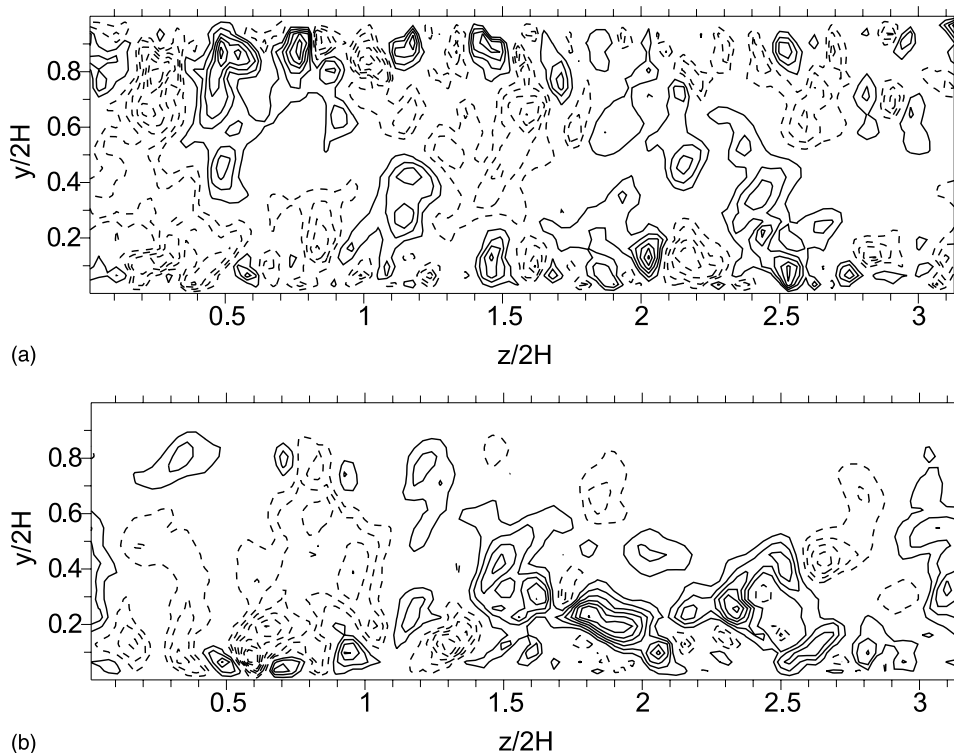


Fig. 10. Contours of secondary flow component  $\tilde{v}$  in the  $(y,z)$ -plane averaged over  $8H/u_\tau$ . Contour levels incremented by  $\pm 0.5$ , starting  $\pm 0.5$ . Dashed contours are negative. (a) Case E; (b) case F.

negative values, respectively. The effects of the inter-particle collisions can be seen obviously. It is found that there are almost no large-scale streamwise vortices near the suction surface both for cases D and F. In the present simulations, large-size vortex pairs in the DNS results of Kristoffersen and Andersson (1993) have not been found. These kinds of vortex pairs may be broken by the particles and their interaction. For the cases with the larger and heavier particles (70  $\mu\text{m}$  particles), the sizes of vortex are larger than that of the cases with the 50  $\mu\text{m}$  particles due to the gravitational effects.

#### 4. Conclusion

This paper examined the turbulence modulation due to dispersed small solid particles in the fully developed rotating channel flows. Three particle sets were applied and the effects of their inter-particle collisions were investigated in detail.

From the analysis of the mean one-dimensional energy spectra, it was found, for the larger and heavier particles in the rotating system, their inter-particle collisions with a hard-sphere model enhance the turbulence kinetic energy. Furthermore, the statistical DNS results also showed that, the inter-particle collisions enhance the fluid turbulence energy in the central region mainly at low wavenumbers; they enhance the fluid turbulence energy in the near-wall regions from low wavenumbers to high wavenumbers. It has also been demonstrated how to transfer turbulence kinetic energy components from the streamwise direction to the others by the inter-particle collisions in a rotating channel.

When particles were large and heavy enough (e.g. 70  $\mu\text{m}$  copper particles), they would contribute to the Reynolds stress budgets directly near the pressure surface due to particle accumulation in this area. Moreover, they had a positive contribution in the vicinity of the pressure surface and negative one little far from it to  $\overline{u^2}$  or  $\overline{v^2}$ , and a negative contribution to  $\overline{uv}$  in the vicinity of the pressure surface. Those may be caused by the frequent inter-particle and particle-wall collisions close to the pressure surface. The dissipation and viscous diffusion were changed consequently by the particles. Without consideration of the inter-particle collisions, the magnitudes of the peaks close to the pressure surface were compressed and their positions were moved away from it, and there was almost no gain or loss near the suction surface compared with the corresponding case considering the inter-particle collisions. Production term  $G_{12}$  due to system rotation played an important role in the  $\overline{uv}$  equation, especially for the cases without consideration of the inter-particle collisions.

#### Acknowledgements

The computer code development and simulations were performed on the NEC SX-4 super-computer at the Computer Center of Osaka University, Japan. The first author thanks the financial support for this study by the Japanese Government (Monbusho) scholarship. This research was partially supported by Japan Society for the Promotion of Science, Grant-in-Aid for Scientific Research, No. 11650175. The authors are grateful to the referees for their constructive comments.

## References

- Bradshaw, P., 1969. The analogy between streamline curvature and buoyancy in turbulent shear flow. *J. Fluid Mech.* 36, 177–191.
- Cambon, C., Benoit, J.P., Shao, L., Jacquin, L., 1993. Stability analysis and direct simulation of rotating turbulence with organized eddies. In: Mazumdar, H.P. (Ed.), *Some Applied Problems in Fluid Mechanics*. Indian Statistical Institute, pp. 125–153.
- Cambon, C., Jacquin, L., 1989. Spectral approach to non-isotropic turbulence subjected to rotation. *J. Fluid Mech.* 202, 295–317.
- Cambon, C., Mansour, N.N., Godeferd, F.S., 1997. Energy transfer in rotating turbulence. *J. Fluid Mech.* 337, 303–332.
- Canuto, V.M., Dubovikov, M.S., 1997. A dynamical model for turbulence. V. The effect of rotation. *Phys. Fluids* 9, 2132–2140.
- Cherukat, P., McLaughlin, J.B., Dandy, D.S., 1999. A computational study of the inertial lift on a sphere in linear shear flow field. *Int. J. Multiphase Flow* 25, 15–33.
- Dennis, S.C.R., Singh, S.N., Ingham, D.B., 1980. The steady flow due to a rotating sphere at low and moderate Reynolds number. *J. Fluid Mech.* 101, 257–279.
- Elghobashi, S., Truesdell, G.C., 1993. On the two-way interaction between homogeneous turbulence and dispersed solid particles. I: Turbulence modification. *Phys. Fluids A* 5, 1790–1802.
- Gore, R., Crowe, C.T., 1989. Effect of particle size on modulating turbulent intensity. *Int. J. Multiphase Flow* 15, 279–285.
- Hall, D., 1988. Measurements of the mean force on a particle near a boundary in turbulent flow. *J. Fluid Mech.* 187, 451–466.
- Halleen, R.M., Johnston, J.P., 1967. The influence of rotation on flow in a long rectangular channel: an experimental study. Department of Mechanical Engineering, Stanford University, Rep. MD-18.
- Hetsroni, G., 1989. Particles–turbulence interaction. *Int. J. Multiphase Flow* 15, 735–747.
- Hinze, J.O., 1975. *Turbulence*. McGraw-Hill, New York.
- Johnston, J.P., Halleen, R.M., Lezius, D.K., 1972. Effects of spanwise rotation on the structure of two-dimensional fully developed turbulent channel flow. *J. Fluid Mech.* 56, 533–557.
- Kim, J., 1983. The effect of rotation on turbulence structure. In: *Proceedings of the 4th Symposium on Turbulent Shear Flows*, Karlsruhe, pp. 6.14–6.19.
- Kim, J., Moin, P., 1985. Application of a fractional-step method to incompressible Navier–Stokes equations. *J. Comput. Phys.* 59, 308–323.
- Kim, J., Moin, P., Moser, M.D., 1987. Turbulence statistics in fully developed channel flow at low Reynolds number. *J. Fluid Mech.* 177, 133–166.
- Kristoffersen, R., Andersson, H.I., 1993. Direct simulations of low-Reynolds-number turbulent flow in a rotating channel. *J. Fluid Mech.* 256, 163–197.
- Kulick, J.D., Fessler, J.R., Eaton, J.K., 1994. Particle response and turbulence modification in fully developed channel flow. *J. Fluid Mech.* 277, 109–134.
- Lezius, D.K., Johnston, J.P., 1976. Roll-cell instabilities in rotating laminar and turbulent channel flows. *J. Fluid Mech.* 77, 153–175.
- Maxey, M.R., Riley, J.J., 1983. Equation of motion for a small rigid sphere in nonuniform flow. *Phys. Fluids* 26, 883–889.
- McLaughlin, J.B., 1994. Numerical computation of particles–turbulence interaction. *Int. J. Multiphase Flow* 20 (Suppl.), 211–232.
- Miyake, Y., Kajishima, T., 1986a. Numerical simulation of the effects of Coriolis force on the structure of turbulence. Global effects. *Bull. JSME* 29, 3341–3346.
- Miyake, Y., Kajishima, T., 1986b. Numerical simulation of the effects of Coriolis force on the structure of turbulence. Structure of turbulence. *Bull. JSME* 29, 3347–3351.
- Moin, P., Kim, J., 1982. Numerical investigation of turbulent channel flow. *J. Fluid Mech.* 118, 341–377.
- Moser, R.D., Moin, P., 1987. The effects of curvature in wall-bounded turbulent flows. *J. Fluid Mech.* 175, 479–510.

- Pan, Y., Banerjee, S., 1997. Numerical investigation of the effects of large particles on wall-turbulence. *Phys. Fluids* 9, 3786–3807.
- Pan, Y.-K., Tanaka, T., Tsuji, Y., 2000. Large-eddy simulation of particle-laden rotating channel flows. ASME FEDSM2000-11144, Boston, USA.
- Pan, Y.-K., Tanaka, T., Tsuji, Y., 2001a. Direct numerical simulation of particle-laden rotating channel flow. *Phys. Fluids* 13, 2320–2337.
- Pan, Y.-K., Tanaka, T., Tsuji, Y., 2001b. Numerical study of particle laden rotating turbulence. In: Proceedings of the 4th International Conference on Multiphase Flow (ICMF-2001), New Orleans, USA.
- Rubinow, S.I., Keller, J.B., 1961. The transverse force on a spinning sphere moving in a viscous fluid. *J. Fluid Mech.* 11, 447–459.
- Saffman, P.G., 1965. The lift on a small sphere in a slow shear flow. *J. Fluid Mech.* 22, 385–400.
- Saffman, P.G., 1968. Corrigendum to “The lift on a small sphere in a slow shear flow”. *J. Fluid Mech.* 31, 624.
- Schiller, L., Naumann, A., 1933. *V.D.I. Zeits.* 77, 318–320 (cited in Clift, Grace, & Weber, 1978).
- Spalart, P.R., Moser, R.D., Rogers, M.M., 1991. Spectral methods for the Navier–Stokes equations with one infinite and two periodic directions. *J. Comput. Phys.* 96, 297–324.
- Squires, K.D., Eaton, J.K., 1990. Particle response and turbulence modification in isotropic turbulence. *Phys. Fluids A* 2, 1191–1203.
- Sundaram, S., Collins, L.R., 1994a. Spectrum of density fluctuations in a particle–fluid system I. Monodisperse spheres. *Int. J. Multiphase Flow* 20, 1021–1037.
- Sundaram, S., Collins, L.R., 1994b. Spectrum of density fluctuations in a particle–fluid system II. Polydisperse spheres. *Int. J. Multiphase Flow* 20, 1039–1052.
- Sundaram, S., Collins, L.R., 1999. A numerical study of the modulation of isotropic turbulence by suspended particles. *J. Fluid Mech.* 379, 105–143.
- Tabakoff, W., 1984. Review-turbomachinery performance deterioration exposed to solid particulates environment. *ASME J. Fluid Eng.* 106, 125–134.
- Takagi, H., 1977. Viscous flow induced by slow rotation of a sphere. *J. Phys. Soc. Jpn.* 42, 319–325.
- Tanaka, T., Tsuji, Y., 1991. Numerical simulation of gas–solid two-phase flow in a vertical pipe: on the effect of inter-particle collision. In: *ASME/FED Gas–Solid Flows*, pp. 123–128.
- Tritton, D.J., 1992. Stabilization and destabilization of turbulent shear flow in a rotating fluid. *J. Fluid Mech.* 241, 503–523.
- Tsuji, Y., 1984. *Pneumatic Conveying*. Nikkann, Kogyo (in Japanese).
- Tsuji, Y., 1991. Review: Turbulence modification in fluid–solid flows. In: Stock, D.E., et al. (Eds.), *Gas–Solid Flows*, ASME-FED, vol. 110, pp. 1–6.
- Yarin, L.P., Hetsroni, G., 1994. Turbulence intensity in dilute two-phase flows – 3. The particles–turbulence interaction in dilute two-phase flow. *Int. J. Multiphase Flow* 20, 27–44.
- Yeung, P.K., Zhou, Y., 1998. Numerical study of rotating turbulence with external forcing. *Phys. Fluids* 10, 2895–2909.
- Yuan, Z., Michaelides, E.E., 1992. Turbulence modulation in particulate flows – a theoretical approach. *Int. J. Multiphase Flow* 18, 779–785.
- Zhou, Y., 1995. A phenomenological treatment of rotating turbulence. *Phys. Fluids* 7, 2092–2094.